Spontaneous Tilt of Single-Clamped Thermal Elastic Sheets

Zhitao Chen,[1] Duanduan Wan,[2] and Mark J. Bowick[3,*]
[1]Department of Physics, University of California Santa Barbara, Santa Barbara, California 93106, USA
[2]School of Physics and Technology, Wuhan University, Wuhan 430072, China
[3]Kavli Institute for Theoretical Physics, University of California Santa Barbara, Santa Barbara, California 93106, USA

(Received 5 May 2021; accepted 24 December 2021; published 14 January 2022)

Very thin elastic sheets, even at zero temperature, exhibit nonlinear elastic response by virtue of their dominant bending modes. Their behavior is even richer at finite temperature. Here, we use molecular dynamics to study the vibrations of a thermally fluctuating two-dimensional elastic sheet with one end clamped at its zero-temperature length. We uncover a tilted phase in which the sheet fluctuates about a mean configuration inclined with respect to the horizontal, thus breaking reflection symmetry. We determine the phase behavior as a function of the aspect ratio of the sheet and the temperature. We show that tilt may be viewed as a type of transverse buckling instability induced by clamping coupled to thermal fluctuations and develop an analytic model that predicts the tilted and untilted regions of the phase diagram. Qualitative agreement is found with the molecular dynamics simulations. Unusual response driven by control of purely geometric quantities like the aspect ratio, as opposed to external fields, offers a very rich playground for two-dimensional mechanical metamaterials.

DOI: 10.1103/PhysRevLett.128.028006

Elastic sheets and cantilever ribbons have long been studied in classical plate theory [1,2]. The energetic cost of elastic stretching relative to the bending, escape into the third dimension through height fluctuations, is controlled by the dimensionless Föppl-von Kármán number $\mathrm{vK} \sim A/t^2$, where A is the area of the sheet and t is the thickness. In the very thin limit, such as atomically thin graphene, bending dominates and vK may be tuned by varying purely geometric scales rather than external fields. The mechanical behavior of thin sheets is even richer when they are thermalized [3,4]. Instead of always crumpling, like linear polymer chains, thermal excitations lead to a low-temperature wrinkled flat phase, even for arbitrarily large sheets. In the wrinkled phase, the bending rigidity and elastic moduli become scale-dependent rather than simple material parameters (see, e.g., Refs. [5–14]). In particular the renormalized bending rigidity κ_R is strongly scale-dependent, with an enhancement over the zero-temperature value κ by a factor $(L/l_{\mathrm{th}})^{\eta}$, where L is the smallest 2D spatial extent of the sheet, say the length L, and l_{th} is the length scale above which the effect of thermal fluctuations becomes significant, with the critical exponent η being approximately 0.8 (e.g., Refs. [9,15–19]). The crucial length l_{th} is given by $l_{\mathrm{th}} = \sqrt{16\pi^3\kappa^2/3k_BTY}$, where Y is the zero-temperature value of the Young's modulus. This almost linear enhancement allows for further geometric tuning of the thermalized mechanical response, especially since the room temperature thermal length scale is of order nanometers or less for strong covalently bonded materials such as graphene [20,21]. This is a result of both small bending rigidity and large Young's modulus. For soft membranes both κ and Y are small, which means the thermal length scale often exceeds the physical size of the system and thermal effects are irrelevant. The combination of thermal fluctuations and geometric control provides a rich toolbox for generating unusual behavior.

Recently, the field has advanced considerably with the experimental observations in Ref. [20], who studied the deflections and thermal fluctuations of atomically thin, 10 μm wide freestanding graphene cantilevers and springs, and found a renormalized bending rigidity at room temperature of order 4000 times larger than its microscopic value at $T = 0$. This remarkable enhancement of the bending rigidity is consistent with the predicted stiffening due to thermal fluctuations alone. The predicted softening of the in-plane Young's modulus [10] of a graphene sheet polymer (by a factor of roughly 25) has also been observed experimentally [21].

The linear and nonlinear mechanical response of thin sheets in cantilever (single-clamp) or double-clamp configurations, possibly decorated with cuts or holes to facilitate escape into the third dimension [20,22,23], is interesting in its own right. One can also envision applications such as nanosprings, nanoscale actuators, nanokirigami, and highly sensitive temperature or mass sensors [24]. To properly design and understand such devices at room temperature, one must explore how thermal fluctuations affect the mechanical properties of individual thin sheets. Theoretically, the thermalized behavior of single-clamped [25] and double-clamped [26] long ribbons has been studied previously, as well as thermalized Euler buckling of the double-clamped system [27]. Buckling

of square and circular elastic sheets has also been explored [14,28,29].

Here, we use molecular dynamics (MD) simulations to study a thermal elastic sheet of zero-temperature width W_0 and length L_0, with the aspect ratio $\alpha = W_0/L_0 \geq 1$, clamped along only one edge of width W_0. We find that besides the horizontal phase where the system vibrates about the horizontal plane, it can also exhibit a tilted phase where the elastic sheet spontaneously tilts, i.e., oscillates about a mean buckled configuration that is tilted with respect to the horizontal. Since the tilt plane is equally likely to be above or below the horizontal plane, we have in fact a 2-state oscillator. We show the phase diagram of the system as a function of the temperature and the aspect ratio. Interestingly, the tilted phase only exists for a finite window of the aspect ratio. Further, we provide a theoretical explanation that qualitatively fits the simulation results. As we will show more precisely later, the combination of thermal fluctuations and clamping deforms the reference thin sheet by a length scale proportional to $(k_B T/\kappa) g(\alpha) L_0$, where g is some function of the aspect ratio. This deformation sets off a competition between in-plane compression and out-of-plane bending, and bending is energetically more favorable if the deformation is larger than a length scale approximately proportional to κ/YL_0. Therefore, we expect a big thin sheet with a small κ and large Y to buckle in our setup at a high temperature for some aspect ratio. This is consistent with the classic intuition that a long, solid but flexible beam is susceptible to buckling under compression. Apart from clamping, no external forces or fields are present in the setup, so our finding identifies a way of controlling the states of 2D materials by pure geometry and temperature.

We model an elastic sheet as a discrete triangular lattice of vertices and bonds, with the elastic energy being a sum of a stretching term and a bending term:

$$E = \frac{\varepsilon}{2} \sum_{\langle ij \rangle} (|\boldsymbol{r}_i - \boldsymbol{r}_j| - a)^2 + \frac{\tilde{\kappa}}{2} \sum_{\langle IJ \rangle} (\hat{\mathbf{n}}_I - \hat{\mathbf{n}}_J)^2, \qquad (1)$$

where ε is the discrete spring constant, a is the equilibrium spring length, and $\tilde{\kappa}$ is the discrete bending modulus. The sum $\langle ij \rangle$ is over pairs of nearest-neighbor vertices, with positions $\boldsymbol{r}_i$ in 3D Euclidean space, while the sum $\langle IJ \rangle$ is over all pairs of triangular plaquettes, with unit normals $\hat{\mathbf{n}}_I$, that share a common edge. The continuum limit of Eq. (1) leads to a Young's modulus $Y = 2\varepsilon/\sqrt{3}$, a bending rigidity $\kappa = \sqrt{3}\tilde{\kappa}/2$, and a Poisson ratio $\nu = 1/3$ [30–32]. For graphene the discrete triangular lattice may be viewed as the dual of its actual honeycomb lattice [26] with edge length $a = \sqrt{3}a_0$, where $a_0 = 1.42$ Å is the carbon-carbon bond length. We use graphene's microscopic material parameters $\kappa = 1.2\,\text{eV}$ [33,34] and $Y = 20\,\text{eV/Å}^2$ [35,36]. Figure 1(a) displays the zero-temperature flat configuration

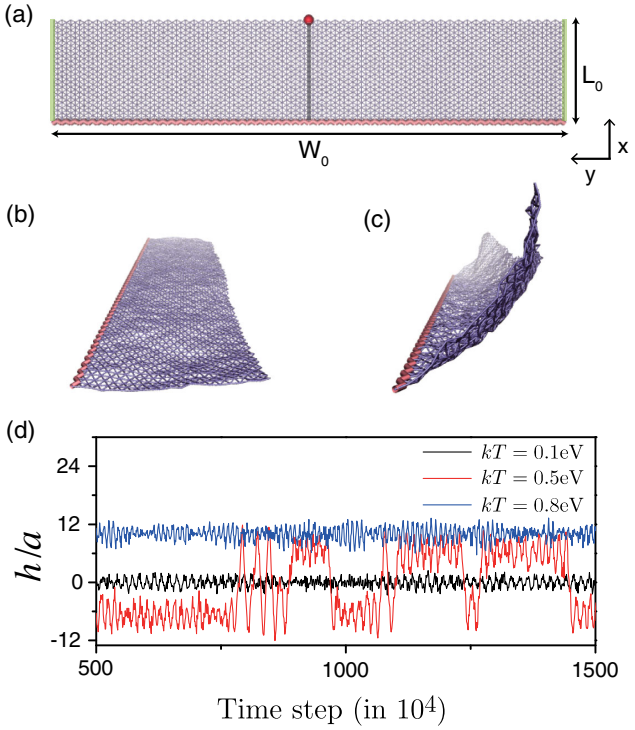

FIG. 1. (a) A triangulated membrane with zero-temperature length $L_0 = 20a$ and aspect ratio $\alpha = W_0/L_0 \approx 5$ clamped on the back edge (colored pink). The middle vertex on the front edge is marked with a large red dot. We label the left and right edges in green and the centerline in gray. The snapshot was generated using the visual molecular dynamics package [41] and rendered using the Tachyon ray tracer [42]. (b) Snapshot of the horizontal phase. (c) Snapshot of the tilted phase. (d) Height (measured in the zero-temperature lattice spacing a) of the red vertex as a function of time for 10^6 time steps after equilibrating for 5×10^6 time steps.

of a sheet in the x-y plane, with $L_0 = 20a \approx 50$ Å and aspect ratio $\alpha = W_0/L_0 \approx 5$, where the subscript 0 labels zero-temperature quantities. We clamp the edge vertices along one zigzag boundary indicated by the pink line in Fig. 1(a) and tag the middle vertex on the free end (shown in red). We find consistent results from MD simulations using two different software packages: HOOMD-blue [37,38] and LAMMPS [39]. After giving the free vertices a small random out-of-plane displacement, we update their positions with the Nosé-Hoover thermostat, in which the system reaches a target temperature and evolves in the constant temperature ensemble (see the Supplemental Material for details [40]). Every simulation run consists of 10^7 time steps in total, with the first 5×10^6 time steps ensuring equilibrium.

Our system exhibits two phases depending on the aspect ratio and the temperature: a horizontal phase where the sheet vibrates about the horizontal $z = 0$ plane, and a tilted phase where it vibrates about a tilted configuration. We show snapshots of the two phases in Figs. 1(b) and 1(c).

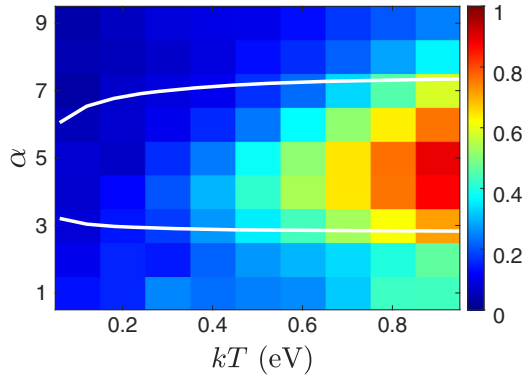

FIG. 2. The value of order parameter ϕ as a function of temperature and aspect ratio α. The diagram is obtained by analyzing the second 5×10^6 time steps and averaging over five independent runs. White lines indicate the estimated phase boundary by solving $\Delta_m = \Delta_c$, which are described in Eqs. (5) and (7), respectively.

It is revealing to plot the height h (z coordinate) of the middle vertex of the free long edge [the red vertex in Fig. 1(a)] for 10^6 time steps after equilibrating—see Fig. 1(d). At low temperature ($kT = 0.1$ eV), the red vertex vibrates about $z = 0$ (black line). At a higher temperature ($kT = 0.8$ eV), however, the vertex vibrates about $z \approx 10$—the upper trace (blue line). At an intermediate temperature ($kT = 0.5$ eV), the vertex vibrates about two symmetric positions $z \approx \pm 7$ with occasional inversions (red line).

We quantify tilt with an order parameter $\phi \equiv \langle |h/x| \rangle$, where h and x are coordinates of the aforementioned vertex, and the bracket denotes an average over time and independent runs. We plot ϕ as a function of aspect ratio α and temperature kT in Fig. 2, where we have averaged over five independent runs. At sufficiently high temperature and in a moderate range of aspect ratios, the sheet is clearly tilted; otherwise the sheet is horizontal. We do not observe any abrupt discontinuity in Fig. 2, which suggests that the transition between the horizontal phase and the tilted phase is continuous. For a system with an aspect ratio in the window for tilt, the free energy gradually changes from having only one global minimum (horizontal phase) to having two equal local minima (tilt up and tilt down) as temperature increases. A further increase in temperature will lead to the system tilting higher and staying in the tilted state longer. A close look at a typical tilt configuration shows that the sheet is not uniformly tilted along the width direction. We plot the profile of the sheet in the tilted phase in Fig. 3(a), and the two short free edges [marked in green in Fig. 1(a)] and the parallel middle line [marked in gray in Fig. 1(a)] in Fig. 3(b). It can be seen that the middle line has a pronounced buckled profile, while the two free edges have lower curvatures.

The tilted phase may be understood as a result of a buckling instability: a macroscopically flat thermalized

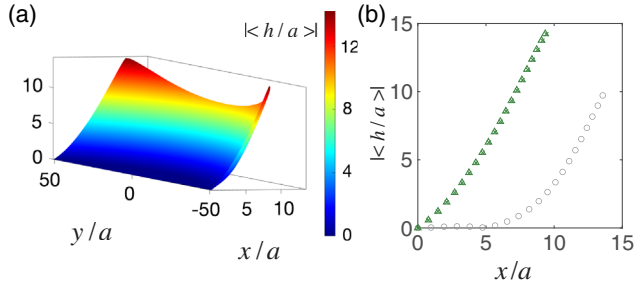

FIG. 3. A tilted membrane with $kT = 0.8$ eV and $\alpha = 5$. (a) Interpolated profile of the membrane. (b) Profile of the two short free edges with green crosses and triangles [marked green in Fig. 1(a)] and the parallel middle line with gray circles [marked gray in Fig. 1(a)].

membrane has a projected area smaller than its zero-temperature area due to thermally induced microscopic wrinkles (e.g., Refs. [10,26]). The natural reference state for defining stresses and strains is the thermalized membrane. Thus, clamping one end at its zero-temperature width W_0 exerts a stretching force along the clamped boundary. A combination of stretching and clamped boundaries is known to produce a region of compressive stress in the direction transverse to stretching, leading to a wrinkling instability in double-clamped thin sheets [43–45]. In our case, a similar instability appears as tilting.

To develop an analytic model for tilt (see the Supplemental Material [40] for details about the model), we use the thermalized elastic sheet as our reference state and choose the coordinates such that the thermalized sheet occupies the region $0 \le x \le L'$ and $-W'/2 \le y \le W'/2$ and is clamped at $x = 0$. As discussed above, a thermalized sheet is smaller than its zero-temperature counterpart, so $W' < W_0$ and $L' < L_0$. The deformation from the reference state is described by in-plane displacements $u_x(\boldsymbol{r})$ and $u_y(\boldsymbol{r})$, and an out-of-plane deflection $h(\boldsymbol{r})$. The elastic energy of the system is [46]

$$E = \int d^2 r \left[\frac{\kappa_R}{2} (\nabla^2 h)^2 + \mu_R u_{ij}^2 + \frac{1}{2} \lambda_R u_{kk}^2 \right], \qquad (2)$$

where the strain tensor $u_{ij} = \frac{1}{2}[(\partial u_i/\partial x_j) + (\partial u_j/\partial x_i) + (\partial h/\partial x_i)(\partial h/\partial x_j)]$. Thermal fluctuations renormalize the elastic moduli so that they become (strongly) scale-dependent [5,7–10,47]: $\kappa_R(L_0) \sim \kappa(L_0/l_{\rm th})^{\eta}$ and $Y_R(L_0) = [4\mu_R(\mu_R + \lambda_R)/(2\mu_R + \lambda_R)] \sim Y(L_0/l_{\rm th})^{-\eta_u}$, where $\eta \approx 0.8$ and $\eta_u \approx 0.4$. Clamping imposes a boundary condition $u_x(0, y) = 0$. It also fixes the left edge to the zero-temperature width $W_0 > W'$, imposing stretching on the reference state:

$$u_y\left(0, \frac{W'}{2}\right) = -u_y\left(0, -\frac{W'}{2}\right) = \frac{W_0 - W'}{2} \equiv \frac{\epsilon}{2} W_0. \qquad (3)$$

The extension ratio $\epsilon = (W_0 - W')/W_0$ is approximately given by [10]

$$\epsilon \approx \frac{1}{8\pi}\frac{k_B T}{\kappa}[\eta^{-1} - \eta^{-1}(l_{\rm th}/L_0)^{\eta} + \ln(l_{\rm th}/a)]. \quad (4)$$

We find it useful to double our system to the region $-L' \le x \le L'$ and $-W'/2 \le y \le W'/2$ by reflecting it about the y axis. The originally clamped edge is no longer on the boundary in this doubled system, and $u_x(0, y) = 0$ is automatically satisfied by symmetry. We consider a narrow strip with length $2L'$ around $y = 0$ and call it the middle strip, which can buckle under enough compression and is a simple proxy for the system in our analysis. To determine the compression Δ_m of the middle strip we examine the system from its horizontal ($h = 0$) phase in Eq. (2). The energy functional gives the equilibrium equation for the in-plane stress $\partial_i \sigma_{ij} = 0$ [46].

On the left and right edges of the doubled system, we impose the strong traction-free boundary condition $\sigma_{xx}(\pm L', y) = 0$ and a weak boundary condition $\int \sigma_{xy}(\pm L', y)dy = 0$. On the top and bottom edges we impose $\sigma_{xy}(x, \pm W'/2) = 0$ and $\sigma_{yy}(x, \pm W'/2) = f\cos(\pi x/2L')$, which models the stretching effect from clamping on the reference state. For simplicity, we have used a delocalized stress σ_{yy} instead of a highly localized stress at $x = 0$, and f is determined self-consistently by condition Eq. (3) on the displacement. This set of boundary conditions allows us to solve for the in-plane stress analytically with the Airy stress function method, which confirms that the middle strip is indeed under a compressive stress σ_{xx}.

After applying the stress-strain relation, we obtain $u_{xx}(x, 0)$, which we integrate to obtain the compression Δ_m of the middle strip at $y = 0$. To first order in small ϵ we find

$$\begin{aligned}\Delta_m &= -2u_x(L', 0) \\ &= \frac{L_0\alpha\epsilon}{2\sinh^2(\frac{\pi\alpha}{4})}\left[\frac{\pi\alpha}{4}\cosh\left(\frac{\pi\alpha}{4}\right)(1+\nu_R)\right. \\ &\quad \left. - \sinh\left(\frac{\pi\alpha}{4}\right)(1-\nu_R)\right], \end{aligned} \quad (5)$$

where $\nu_R = \lambda_R/(2\mu_R + \lambda_R)$ is the renormalized Poisson ratio, which would be $-1/3$ for an infinitely sized, freestanding thermalized sheet [9,47]. We observe that Δ_m crosses from negative to positive at some threshold aspect ratio (Fig. 4). This is due to two competing effects. The tensile stress σ_{yy} from clamping tends to extend the middle strip because of an overall negative Poisson ratio of the reference state. The compressive stress σ_{xx}, in contrast, tends to compress the middle strip. Our calculation shows

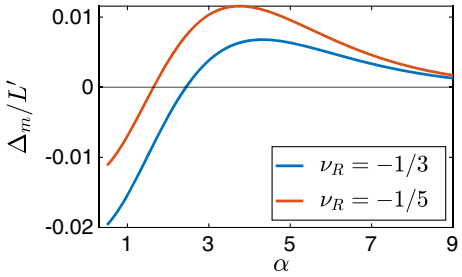

FIG. 4. Compression of middle strip Δ_m/L' as a function of aspect ratio α using Eq. (5), with $\epsilon = 0.05$ and two different renormalized Poisson ratios.

that the former dominates for small aspect ratio, extending the middle strip ($\Delta_m < 0$), and the latter dominates for higher aspect ratios, allowing buckling for a window of aspect ratios. Here, we have ignored all effects of thermal fluctuation besides renormalization of the elastic moduli. A finite element calculation in the same spirit using the FENICS package [48] and a comparison between MD simulation, theory, and finite element calculation is presented in the Supplemental Material [40].

To estimate the critical compression Δ_c above which the sheet buckles, we use a one-dimensional model for the middle strip. Dropping the y derivatives and u_y in Eq. (2), we have an energy density functional $\mathcal{E}[u_x, h] = (\kappa_R/2)\int dx(d^2h/dx^2)^2 + [Y_R/2(1-\nu_R^2)]\int dx[(du_x/dx) + \frac{1}{2}(dh/dx)^2]^2$ with the antiperiodic boundary condition on the displacement $u_x(-L') = -u_x(L') = \Delta/2$. Integrating out the displacement field gives an effective energy density in terms of h alone [40]:

$$\begin{aligned}\mathcal{E}_{\rm eff}[h] &= -\log\left[\int Du_x e^{-\mathcal{E}[u_x,h]}\right] \\ &= \frac{\kappa_R}{2}\int dx\left(\frac{d^2h}{dx^2}\right)^2 \\ &\quad + \frac{Y_R}{4L'(1-\nu_R^2)}\left[\Delta - \frac{1}{2}\int_{-L'}^{L'} dx\left(\frac{dh}{dx}\right)^2\right]^2 \\ &= \frac{\kappa_R}{2}\int dx\left(\frac{d^2h}{dx^2}\right)^2 - \frac{Y_R}{2(1-\nu_R^2)}\frac{\Delta}{2L'}\int dx\left(\frac{dh}{dx}\right)^2 \\ &\quad + \frac{Y_R}{2(1-\nu_R^2)}\frac{1}{8L'}\int\int dxdx'\left(\frac{dh}{dx}\right)^2\left(\frac{dh}{dx'}\right)^2, \end{aligned} \quad (6)$$

where we drop a constant term independent of h from the second line. This can be generalized to a circular plate [29]. We use a mean field variational function $h(x) = H\cos(\pi x/2L')$, where H serves as the buckling order parameter. If minimization of Eq. (6) requires $H = 0$, the strip will stay in the plane; if it requires $H \neq 0$, then the strip will buckle out of the plane. It thus yields a critical compression:

$$\Delta_c = \frac{\pi^2}{2L'}\frac{\kappa_R(1-\nu_R^2)}{Y_R}. \quad (7)$$

Setting $\Delta_m = \Delta_c$, a combination of Eqs. (4), (5), and (7), gives the phase boundary between the horizontal and tilted phases and is shown with thick white lines in Fig. 2. The result shows that the tilted phase exists for a finite window of aspect ratios, consistent with our MD simulations. Here, we have used a constant $\nu_R = -1/3$, which is the universal Poisson ratio for an infinitely sized thermal sheet [9,47]. Finite-size effects and the suppression of thermal fluctuations from clamping may shift ν_R to a less negative value and even introduce spatial and strain dependence. As can be seen from Fig. 4, a less negative Poisson ratio such as $\nu_R = -1/5$ would reduce the effect of the tensile σ_{yy} and favor compression of the middle strip. Our study shows that the compressive stress induced by thermal fluctuation and clamped boundary can overcome a negative Poisson's effect and lead to buckling.

The observation that tilt is only present for $kT \gtrsim 0.4$ eV in MD simulations is a nonuniversal result of the small system size, and we expect that larger systems favor tilt. Equation (5) gives $\Delta_m \sim L_0$, and Eq. (7) gives $\Delta_c \sim L_0^{-1+\eta+\eta_u} \approx L_0^{0.2}$. The amount of compression of the middle strip therefore grows much faster than the critical compression required for tilting as system size increases. A comparison of the phase diagrams of $L_0 = 20a$ and $L_0 = 30a$ suggests that tilt is more easily observed for larger systems [40]. We also observe tilt with $L_0 = 60a$, $\alpha = 5$ at $k_BT = 0.1$ eV, with an order parameter $\phi \approx 0.47$. We expect a much lower tilt temperature for real experiments with larger samples. We hope our work will stimulate experiments that exploit geometric control of mechanical behavior of thermalized 2D metamaterials or other realizations of thermalized elastic sheets.

Z. C. and D. W. contributed equally to this work. The authors thank Rastko Sknepnek for collaboration at the beginning of this work. M. J. B. thanks David R. Nelson for many years of discussion on graphene statistical mechanics. Z. C. thanks Christopher Jardine and Paul Hanakata for helpful discussions. This research was supported in part by the National Science Foundation under Grant No. NSF PHY-1748958. D. W. acknowledges the support from the National Natural Science Foundation of China (Grant No. 11904265), the Hubei Provincial Natural Science Foundation (Grant No. 2020CFB670), and the Fundamental Research Funds for the Central Universities (Grant No. 2042020kf0033). Use was made of computational facilities purchased with funds from the National Science Foundation (CNS-1725797) and administered by the Center for Scientific Computing (CSC). The C. S. C. is supported by the California NanoSystems Institute and the Materials Research Science and Engineering Center (MRSEC; NSF DMR 1720256) at UC Santa Barbara.

*Corresponding author.
bowick@kitp.ucsb.edu

[1] R. D. Blevins, *Formulas for Natural Frequency and Mode Shape* (Krieger Publishing Company, Malabar, FL, USA, 1984).
[2] A. W. Leissa, *Vibration of Plates* (National Aeronautics and Space Administration, Washington, D.C., 1969).
[3] D. Nelson, T. Piran, and S. Weinberg, *Statistical Mechanics of Membranes and Surfaces*, 2nd ed. (World Scientific, Singapore, 2004).
[4] M. J. Bowick and A. Travesset, Phys. Rep. **344**, 255 (2001).
[5] D. R. Nelson and L. Peliti, J. Phys. (Paris) **48**, 1085 (1987).
[6] Y. Kantor and D. R. Nelson, Phys. Rev. A **36**, 4020 (1987).
[7] J. A. Aronovitz and T. C. Lubensky, Phys. Rev. Lett. **60**, 2634 (1988).
[8] E. Guitter, F. David, S. Leibler, and L. Peliti, J. Phys. (Paris) **50**, 1787 (1989).
[9] P. Le Doussal and L. Radzihovsky, Phys. Rev. Lett. **69**, 1209 (1992).
[10] A. Košmrlj and D. R. Nelson, Phys. Rev. B **93**, 125431 (2016).
[11] F. Ahmadpoor, P. Wang, R. Huang, and P. Sharma, J. Mech. Phys. Solids **107**, 294 (2017).
[12] P. Le Doussal and L. Radzihovsky, Ann. Phys. (Amsterdam) **392**, 340 (2018).
[13] B. Sajadi, S. van Hemert, B. Arash, P. Belardinelli, P. G. Steeneken, and F. Alijani, Carbon **139**, 334 (2018).
[14] A. Morshedifard, M. Ruiz-Garca, M. J. Abdolhosseini Qomi, and A. Komrlj, J. Mech. Phys. Solids **149**, 104296 (2021).
[15] J.-P. Kownacki and D. Mouhanna, Phys. Rev. E **79**, 040101 (R) (2009).
[16] D. Gazit, Phys. Rev. E **80**, 041117 (2009).
[17] N. Hasselmann and F. L. Braghin, Phys. Rev. E **83**, 031137 (2011).
[18] A. Tröster, Phys. Rev. B **87**, 104112 (2013).
[19] A. Tröster, Phys. Rev. E **91**, 022132 (2015).
[20] M. K. Blees, A. W. Barnard, P. A. Rose, S. P. Roberts, K. L. McGill, P. Y. Huang, A. R. Ruyack, J. W. Kevek, B. Kobrin, D. A. Muller, and P. L. McEuen, Nature (London) **524**, 204 (2015).
[21] R. J. Nicholl, H. J. Conley, N. V. Lavrik, I. Vlassiouk, Y. S. Puzyrev, V. P. Sreenivas, S. T. Pantelides, and K. I. Bolotin, Nat. Commun. **6**, 8789 (2015).
[22] E. R. Russell, R. Sknepnek, and M. Bowick, Phys. Rev. E **96**, 013002 (2017).
[23] D. Yllanes, S. S. Bhabesh, D. R. Nelson, and M. J. Bowick, Nat. Commun. **8**, 1381 (2017).
[24] K. L. Ekinci and M. L. Roukes, Rev. Sci. Instrum. **76**, 061101 (2005).
[25] M. J. Bowick, A. Košmrlj, D. R. Nelson, and R. Sknepnek, Phys. Rev. B **95**, 104109 (2017).
[26] D. Wan, D. R. Nelson, and M. J. Bowick, Phys. Rev. B **96**, 014106 (2017).
[27] P. Z. Hanakata, S. S. Bhabesh, M. J. Bowick, D. R. Nelson, and D. Yllanes, Extreme Mech. Lett. **44**, 101270 (2021).
[28] P. Le Doussal and L. Radzihovsky, Phys. Rev. Lett. **127**, 015702 (2021).
[29] S. Shankar and D. R. Nelson, Phys. Rev. E **104**, 054141 (2021).

[30] H. S. Seung and D. R. Nelson, Phys. Rev. A **38**, 1005 (1988).
[31] J. Lidmar, L. Mirny, and D. R. Nelson, Phys. Rev. E **68**, 051910 (2003).
[32] B. Schmidt and F. Fraternali, J. Mech. Phys. Solids **60**, 172 (2012).
[33] R. Nicklow, N. Wakabayashi, and H. G. Smith, Phys. Rev. B **5**, 4951 (1972).
[34] A. Fasolino, J. H. Los, and M. I. Katsnelson, Nat. Mater. **6**, 858 (2007).
[35] C. Lee, X. Wei, J. W. Kysar, and J. Hone, Science **321**, 385 (2008).
[36] H. Zhao, K. Min, and N. R. Aluru, Nano Lett. **9**, 3012 (2009).
[37] J. A. Anderson, J. Glaser, and S. C. Glotzer, Comput. Mater. Sci. **173**, 109363 (2020).
[38] J. Glaser, T. D. Nguyen, J. A. Anderson, P. Lui, F. Spiga, J. A. Millan, D. C. Morse, and S. C. Glotzer, Comput. Phys. Commun. **192**, 97 (2015).
[39] S. Plimpton, J. Comput. Phys. **117**, 1 (1995).
[40] See Supplemental Material at http://link.aps.org/supplemental/10.1103/PhysRevLett.128.028006 for movies and details.
[41] W. Humphrey, A. Dalke, and K. Schulten, J. Mol. Graphics **14**, 33 (1996).
[42] J. E. Stone, Master's thesis, Computer Science Department, University of Missouri-Rolla, 1998.
[43] N. Friedl, F. Rammerstorfer, and F. Fischer, Comput. Struct. **78**, 185 (2000).
[44] E. Cerda and L. Mahadevan, Phys. Rev. Lett. **90**, 074302 (2003).
[45] M. Xin and B. Davidovitch, arXiv:2012.13046.
[46] L. D. Landau and E. M. Lifshitz, *Theory of Elasticity*, 3rd ed. (Butterworth-Heinemann, Singapore, 1999).
[47] M. J. Bowick, S. M. Catterall, M. Falcioni, G. Thorleifsson, and K. N. Anagnostopoulos, J. Phys. I France **6**, 1321 (1996).
[48] A. Logg, K.-A. Mardal, and G. Wells, *Automated Solution of Differential Equations by the Finite Element Method: The FEniCS Book* (Springer Publishing Company, Incorporated, New York, 2012).